Annals of Glaciology

Article

Cite this article: Tian L, Gao Y, Weissling B, Ackley SF (2020). Snow-ice contribution to the structure of sea ice in the Amundsen Sea, Antarctica. *Annals of Glaciology* **61**(83), 369–378. https://doi.org/10.1017/aog.2020.55

Received: 5 October 2019
Revised: 22 June 2020
Accepted: 23 June 2020
First published online: 23 July 2020

Keywords:
Ice core; mass-balance reconstruction; sea ice; sea-ice growth and decay; snow and ice chemistry

Author for correspondence:
Stephen F. Ackley,
E-mail: Stephen.Ackley@utsa.edu

cambridge.org/aog

Snow-ice contribution to the structure of sea ice in the Amundsen Sea, Antarctica

Lijun Tian[1], Yongli Gao[1], Blake Weissling[2] and Stephen F. Ackley[2]

[1]Center for Water Research, Department of Geological Sciences, University of Texas at San Antonio, San Antonio, TX, USA and [2]Center for Advanced Measurements in Extreme Environments, University of Texas at San Antonio, San Antonio, TX, USA

Abstract

The widespread occurrence of snow-ice formation on the pack ice plays a critical role in the mass balance of Antarctic sea ice. The stable isotope composition, ice texture and salinity of eight ice cores, obtained from the Amundsen Sea during the Oden Southern Ocean 2010/11 expedition from late December 2010 to January 2011, were investigated to illustrate the snow-ice growth process and its contribution to sea-ice development. Most previous research has utilized $\delta^{18}O$ as an index tracer to determine the percentages of core length that contain meteoric water, i.e. snow ice. However, this standard practice of snow-ice identification might be biased due to normally low-resolution isotopic measurements and mixing/diffusion processes between the snow ice and underlying ice layers. Snow-ice contributions in these ice cores based instead on an updated isotope mixing model are also presented. Depth profiles of ice texture and salinity are described to serve as representations of the structures of these ice cores. Our isotope mixing model produced an average of 15.9% snow-ice contribution for pack ice in the Amundsen Sea, and meteoric water occupying 40% of snow-ice mass for all ice stations. These results are compared to previous investigations of snow-ice occurrence around Antarctica.

Introduction

When the snowpack on sea ice is heavy and thick enough to depress the top surface below sea level, a slush layer or slurry is formed through the mixture of seawater or brine and snow at the base of the snow cover. The snow ice is incorporated into the ice cover after subsequent periods of freezing. In the Antarctic, overall higher snow accumulation on thinner sea ice results in the widespread occurrence of surface flooding and snow-ice formation (Jeffries and others, 1994; Massom and others, 2001). The snow-ice formation on the pack ice plays a critical role in the mass and energy balance of Antarctic sea ice (Arrigo and others, 1997; Maksym and Markus, 2008). The snow-ice formation is also an essential factor for biological productivity within the ice by controlling brine and nutrient flux from seawater to the flooded layer and ice layer below (Ackley and Sullivan, 1994; Fritsen and others, 1994). Lack of knowledge about the snow-ice contribution in Antarctic sea ice could hinder accurate estimates of sea-ice thickness and snow cover depth using remote sensing (Drinkwater and Lytle, 1997; Xie and others, 2013).

After snow ice is integrated into the sea-ice column, it becomes troublesome to discriminate the snow ice consistently from granular frazil ice. However, the stark contrast in the isotopic signatures of snow ice and seawater originated ice can help determine contributions of snow ice to the total ice thickness. Previous studies of the snow-ice component utilized the standard practice to identify all granular ice layers with negative isotope signature ($\delta^{18}O < 0$) as snow ice (e.g. Lange and others, 1990; Eicken and others, 1994; Jeffries and others, 1994). However, this procedure to determine the percentages of core length that contain isotopic signatures of meteoric water might be biased due to the normally low-resolution isotopic measurements, with a single isotope value designated for each 10 cm vertical section cut from sea-ice cores. The mixing and diffusion processes during the flooding and refreezing of snow ice might also modify the isotopic signatures of the snow-ice layers (Maksym and Jeffries, 2001). In contrast to previous research deriving percentages of core length that contain snow ice, we applied an updated isotope mixing model to determine snow-ice contribution in the mass balance in an effort to produce more consistent estimates of snow-ice contributions (e.g. Eicken, 1998; Maksym and Jeffries, 2001).

In the Antarctic, sea-ice extent showed an overall gradual increasing trend during the past four decades (Maksym and others, 2012); however, this trend may have reversed during recent years (Parkinson, 2019). The Bellingshausen/Amundsen Sea sector is an anomalous sector of the Southern Ocean, having a 40-year decreasing trend instead, reaching a minimum in 2007, and showing an upward trend since 2007 (Parkinson, 2019). The snow-ice contributions varied spatially in the Antarctic, comprising only 7% of the ice thickness in the Weddell Sea (Lange and others, 1990) to as high as 36% in the northern Bellingshausen/Amundsen Seas (Jeffries and others, 2001). The modeling of snow-ice thickness in the Antarctic produced the thickest snow ice along the coast in the Amundsen Sea (Maksym and Markus, 2008). The observed spatial variations of snow-ice contributions can have several causes including regional differences in: sea-ice extent/thickness; meteorological conditions, i.e. variations in

snow precipitation between different regions; and surface topography affecting snow buildup around roughness elements. There is almost no in situ data available along the southern Amundsen Sea until now, except a few cores obtained by Jefffries and others (1994). Sea-ice cores were collected in the southern Amundsen Sea during the Oden Southern Ocean 2010/11 (OSO1011) expedition from late December 2010 and January 2011 (Fig. 1). In this paper, the measurements of stable isotope variations and ice texture profiles of these ice cores are utilized to delineate snow-ice contribution to ice development in the Amundsen Sea. These results are then compared to previous investigations of snow-ice occurrence around Antarctica.

Materials and methods

Sampling and field measurements

Eight ice stations A2, A5, A6, A7, A8, A9, A10 and A12 were designated during the Amundsen Sea transits A-II, A-V, A-VI, A-VII, A-VIII, A-IX, A-X and A-XII, respectively (Fig. 1). Internal decay features indicate that they are second-year or multiyear ice. While slush layers were observed often at the base of the snowpack, the latest snow-ice formation was unlikely due to the summer conditions for these ice stations at the time of sampling. There was no superimposed ice observed for all ice stations. All ice cores were collected from drifting pack ice, except ice core A12 sampled from fast ice. Sampling information and core description for the eight cores collected are given in Table 1.

Most ice stations had significant components of ridged ice; however, ice cores were acquired on level ice within the station area. Snow depth at our sampling sites was measured using meter sticks. The snow depth at our core sites exhibits strong spatial variability, with a range of 12–72 cm except for only trace snow observed at ice core A2 (Table 1). Negative freeboard was observed at ice stations A5, A6, A7, A8 and A9 due to their relatively high snow-to-ice thickness ratio, while other stations (A2, A10, A12) had positive freeboard. We would investigate if the snow depth is an indicator of the snow-ice contributions in these ice cores later.

Analyses of salinity, ice texture and water isotope ratios

The cores were placed in plastic bags and transferred to a cold room (-40°C) onboard the R/V Oden. Cores were shipped back frozen to the US Army Cold Regions Research and Engineering Laboratory (CRREL) in Hanover, NH. In a cold room there, each core was cut into two halves vertically using a bandsaw. One half core was cut into nominal 10 cm vertical sections, and then the ice sections were melted in separate containers. Salinity was measured with a conductivity probe and meter (Beckman Coulter®) for each melted subsample. A vertical thick section slice (3 mm thickness) was taken from the center of another half core. The ice texture of each thick section (10 cm length) was examined between crossed polaroids on a light table in the cold room. Three ice textures (columnar, granular and mixed columnar/granular) were distinct and distinguishable in these thick sections. Then the thick sections were sealed and melted in plastic ziplock bags at room temperature. Immediately after melting, the meltwater was poured into vials, capped with no headspace, sealed with parafilm and stored in a refrigerator for future water isotope analyses.

A total of 92 melted sea-ice samples from the eight cores (Table 1) were prepared for stable isotope analyses. The δ^{18}O and δD measurements of these samples were performed on a Picarro L2130-i water isotope analyzer (cavity ring-down spectroscopy, CRDS) in the Department of Geological Sciences, University of Texas at San Antonio. Results are reported as relative to the standard Vienna Standard Mean Ocean Water (VSMOW). The measurement precisions for δ^{18}O and δD are 0.1‰ and 0.4‰, respectively. δ^{18}O and δD are given in the following equations:

$$\delta^{18}\mathrm{O} = \frac{[(^{18}\mathrm{O}/^{16}O)_{Sample} - (^{18}\mathrm{O}/^{16}O)_{VSMOW}]}{(^{18}\mathrm{O}/^{16}O)_{VSMOW}} \times 10^3\ ‰ \quad (1)$$

$$\delta D = \frac{[(D/H)_{Sample} - (D/H)_{VSMOW}]}{(D/H)_{VSMOW}} \times 10^3\ ‰ \quad (2)$$

Isotopic approaches to determine snow-ice contributions

Most previous research has only used δ^{18}O as an index tracer to determine the percentages of core length that contain snow ice (e.g. Lange and others, 1990; Eicken and others, 1994; Jeffries and others, 1994). Granular ice could originate from either frazil ice or snow ice, but the stable isotope signal of these layers could demonstrate their origin (Lange and others, 1990). Typically, the granular layers with $\delta^{18}\mathrm{O} < 0$ were assigned as snow ice; while granular layers with $\delta^{18}\mathrm{O} > 0$ were assigned as frazil ice.

However, there are several limitations in such a classification approach that need to be addressed. The brine exchange with ocean must occur through the porous channels when the slush layer is formed at the base of the snow cover; while the flooded layer freezes, the diffusive-convective process would also occur along the ice column during freeze-up of the porous channels (Lange and Hubberten, 1992; Eicken, 1998; Massom and others, 2001). Then the snow-ice layers will tend to lose isotopic signature of snow, while underlying ice layers may become enhanced with snow signature. In addition, the initial freezing process through frazil accumulation could incorporate falling snow particles floating at the sea surface. Thus, the underlying frazil ice sections could then have negative δ^{18}O due to varying degrees of the admixture of snow and seawater isotopic signatures.

The simulated distribution of sea-ice isotopic values, utilizing typical mean and standard deviation of isotope values for seawater and snow ice, should be a bimodal distribution with two peaks (Fig. 2a): one peak is the seawater distribution with higher mean value and smaller variance; one peak is snow-ice distribution with lower mean value and larger variance. The error of snow-ice classification ($\delta^{18}\mathrm{O} < 0$) should be negligible. However, the actual distribution of isotopic values for our 92 sea-ice samples lack the peak of snow ice (Fig. 2b), which suggests significant mixing between the snow ice and seawater originated samples, either due to in situ diffusion process or low-resolution sampling. The classification of many slightly negative δ^{18}O samples, falling between −3‰ and 0‰, as snow-ice layers using the standard practice of snow-ice identification might be problematic.

Snow-ice layers in ice cores as defined by negative δ^{18}O values suggest that the snow or meteoric-water fractions in snow-ice sections could be as low as 10% (Jeffries and others, 2001). However, the model of snow-ice formation implied snow ought to have occupied 30–50% of snow-ice mass during the freezing of a slush layer (Maksym and Jeffries, 2001) utilizing typically observed snow densities (Sturm and others, 1998). The discrepancy between the isotopic approach and model results indicates either that an ice layer with negative δ^{18}O might not be snow ice, or the snow-ice layer became enriched due to the exchange of brine during freezing (Lytle and Ackley, 2001).

Many previous studies tried to determine the snow/meteoric-water fraction within the snow-ice sections or ice cores using an isotope mixing model (Lange and others, 1990; Eicken and others,

https://doi.org/10.1017/aog.2020.55 Published online by Cambridge University Press

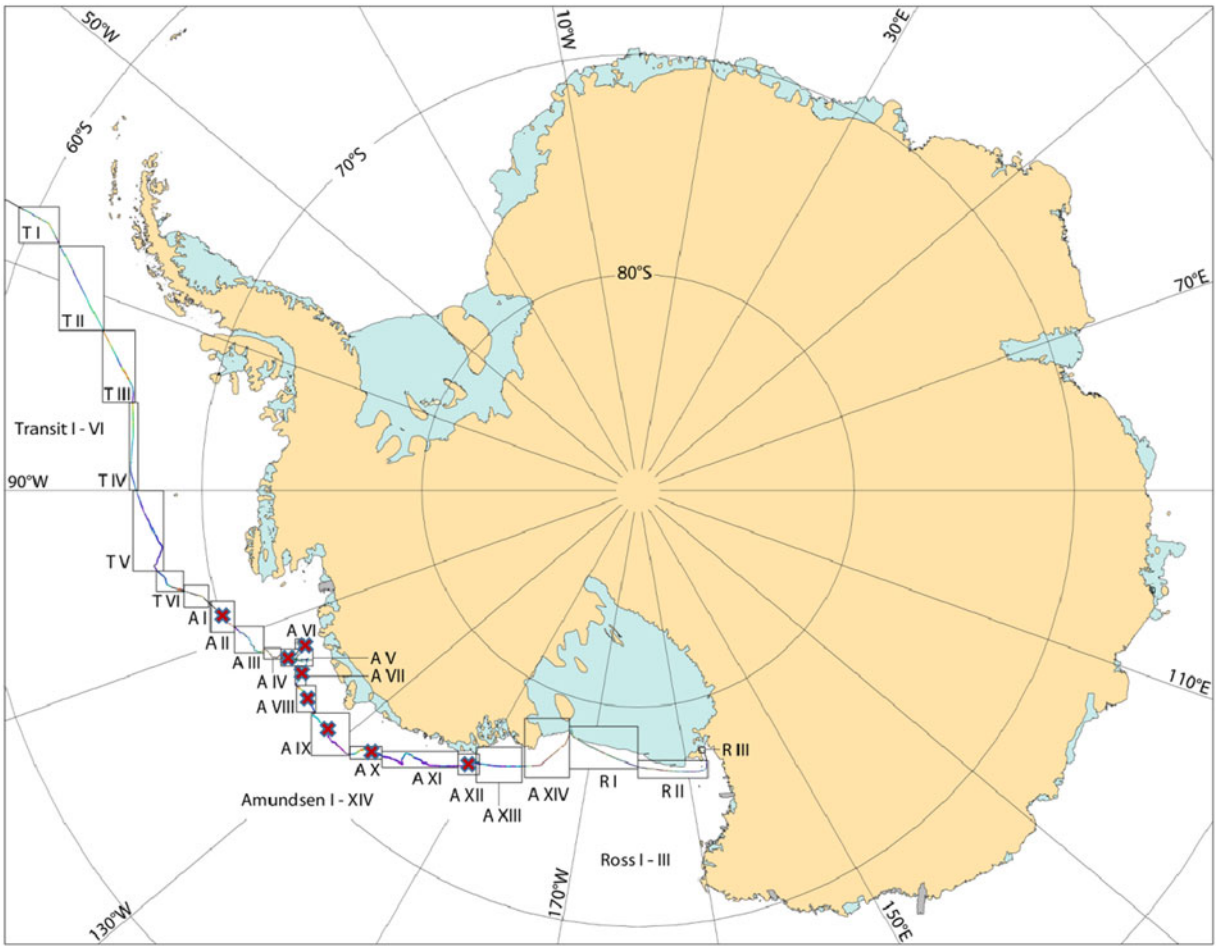

Fig. 1. Oden Southern Ocean 2010/11 expedition track with locations of eight ice stations (red crosses) in the Amundsen Sea. The detailed transit data of the OSO 1011 expedition are available at https://oden.geo.su.se/oso1011. The station locations at the time of sampling were well inside the ice edge (> 50 km) and in areas of greater than 80% ice concentration.

Table 1. Summary of the ice stations with sampling information, core information, snow depth and bulk salinity

Ice core	Date	Location	Core length cm	Subsample numbers	Snow depth cm	Bulk salinity psu
A2	18 December 2010	70.02°S, 106.92°W	73	7	NA	5.0
A5	24 December 2010	71.93°S, 115.13°W	100	10	45	4.1
A6	26 December 2010	72.95°S, 116.91°W	190	19	42	4.1
A7	27 December 2010	72.25°S, 119.04°W	80	8	72	5.8
A8	29 December 2010	72.05°S, 123.12°W	60	6	36	6.2
A9	30 December 2010	72.17°S, 127.06°W	167	17	44	4.7
A10	3 January 2011	72.78°S, 135.59°W	110	11	12	3.4
A12	6 January 2011	75.55°S, 149.29°W	140	14	42	4.9

1994; Jeffries and others, 1994). The ice sections are not a closed system for water isotopes due to brine drainage or convective transport during the snow-ice formation and freezing (Golden and others, 1998). While in an Arctic study (Tian and others, 2018), the hydrochemical characteristics of sea-ice core and seawater depth profiles indicated little snowmelt enters the upper ocean during sea-ice evolution. Since it is not known how much of the meteoric signature in the slush drains into the ocean during freezing in this study, we instead assume that the meteoric signal is 'diffused' through the ice column but not lost to the ocean. In that sense, the whole ice column is considered as a closed system with regard to water isotopes but not brine, which is the primary source of uncertainty in our model.

With assumptions of a similar endmember of snow ice for all ice cores and the mixing process during the snow-ice refreezing, we applied an updated isotope mixing model (one-tracer for two-component) to determine 'snow-ice' contribution in the mass balance for each ice core based on the following equation:

$$\delta^{18}O_{SI}F_{SI} + \delta^{18}O_{SW}(1 - F_{SI}) = \delta^{18}O_{Core} \quad (3)$$

where F_{SI} is the unknown 'snow ice' fraction; $\delta^{18}O_{Core}$ is bulk oxygen isotope value for each ice core; $\delta^{18}O_{SI}$ and $\delta^{18}O_{SW}$ are oxygen isotope values for the 'snow ice' and the 'seawater' components, respectively. The endmembers for $\delta^{18}O_{SI}$ and $\delta^{18}O_{SW}$ would be assigned later for water balance calculations.

The meteoric-water fraction in ice cores could be derived utilizing a similar isotope mixing model (Granskog and others, 2017). We could also calculate the meteoric-water fraction in

https://doi.org/10.1017/aog.2020.55 Published online by Cambridge University Press

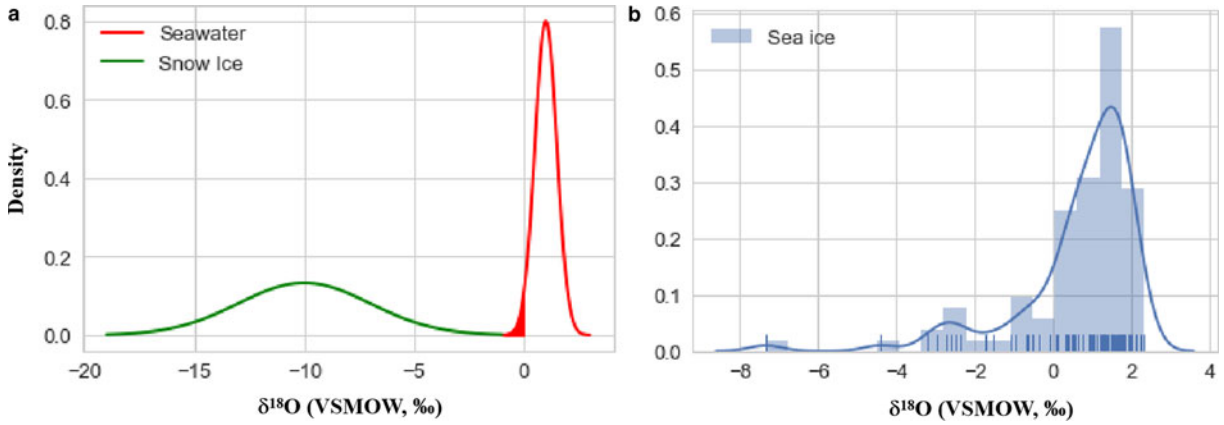

Fig. 2. (a) Simulated distribution of sea-ice samples with typical isotope values for seawater (1 ± 0.5‰) and snow ice (− 10 ± 3‰); (b) actual distribution of isotopic values for 92 sea-ice samples. The shade in Figure 2a was referred to as 'false negatives' which represents the misclassification of snow-ice layers; in Figure 2b, the tick marks on the horizontal axis represent measured isotope values of sea-ice samples, and the blue curve is the kernel density estimation by smoothing the observed density.

our sea-ice cores based on the following equation:

$$\delta^{18}O_M F_M + \delta^{18}O_{SW}(1 - F_M) = \delta^{18}O_{Core} \quad (4)$$

where F_M is the unknown 'meteoric water' fraction; $\delta^{18}O_M$ is oxygen isotope value for the 'meteoric water' component; $\delta^{18}O_{SW}$ and $\delta^{18}O_{Core}$ are the same as those in equation (3). The endmembers for $\delta^{18}O_M$ and $\delta^{18}O_{SW}$ would be assigned later for water balance calculations.

However, there are several caveats in our isotope mixing models: we assume no snowmelt enters the upper ocean during the surface flooding and snow-ice formation; the initial incorporation of snowfall through frazil accumulation is considered limited; the limited sampling of ice cores may not be representative of snow-ice conditions in the Amundsen Sea.

Previous standard classification method identified snow-ice layers for all ice sections, based on the 'prior' information that snow-ice layers have formed in the upper layers of ice cores with negative isotopic signals. The total percentages of core length containing snow ice (P_{SI}) would then be derived from this standard classification method. Our updated isotope mixing model estimated instead the 'posterior' snow-ice contribution (F_{SI}) for the bulk of ice core, considering the whole ice column as a closed system for water isotopes allowing mixing/diffusion processes between ice layers. In this study, we will compare the performance of these two different methods for snow-ice apportionment and explore underlying reasons for the differences among the methods. The meteoric-water fraction (F_M) calculated from equation (4) would be weighed against these two snow-ice apportionment results (P_{SI} and F_{SI}) to check if there is significant initial incorporation of snowfall and/or snowmelt lost to the upper ocean.

Results and discussion

Water isotopes, salinity and texture profiles

The depth profiles of stable oxygen isotope, salinity and ice texture of eight sea ice cores are shown in Figure 3, and the data used in this study can be found in Suppleme ntary Material. $\delta^{18}O$ values for all sea ice samples vary from 2.3‰ to − 7.3‰. Cores A2, A7 and A8 all show low $\delta^{18}O$ signals at the surface portion (0–10 cm); both cores A5 and A6 appear with low $\delta^{18}O$ signal at a relatively greater depth; core A10 shows the low $\delta^{18}O$ signals both at the surface portion and bottom portion; both cores A9 and A12 have generally higher $\delta^{18}O$ signals with no particular pattern. Lack of low $\delta^{18}O$ layers in cores A9 indicates the diffusion and homogenization in the snow-ice refreezing process. There should be no snow-ice formation at fast ice station A12 due to its identical columnar texture and no slush layer observed. Previous isotope measurements (Jeffries and others, 1994) and modeling results (Maksym and Jeffries, 2001) illustrated that negative $\delta^{18}O$ values occurred at the surface then steadily enriched $\delta^{18}O$ values with increasing depth. However, in our study, the possible snow-ice layers with low $\delta^{18}O$ values also occur at some distance below the surface, primarily in granular layers but occasionally in columnar layers. The snow-ice layers below the surface could be a result of prior deformation through the dynamic rafting process; however, the ice layers with slightly negative values are more likely due to mixing and diffusion processes during flooding and refreezing of snow ice.

The salinities for all sea-ice samples vary from 1.7 to 9.5 psu (Fig. 3), while the bulk salinities of all ice cores vary between 3.4 and 6.2 psu (Table 1), which are lower than typical salinity of first-year sea ice. The low salinity could happen in thicker first-year ice or typical multiyear ice. In our study, the pack ice stations (except A12) might be first-year ice that has survived through much of the current summer, and they would be second-year ice soon. The salinity profiles show significant negative correlations with $\delta^{18}O$ profiles in most ice cores, for the reason that snow-ice layers with low $\delta^{18}O$ signals generally have higher salinities. However, salinity is not a good indicator of provenance for sea-ice layers.

There are three different classes of ice textures: columnar (n = 27), granular (n = 48), mixed columnar/granular (n = 17). The eight cores show variable contributions of granular ice from 0 to 100% of the total length of these cores (Fig. 3), with an average of 52%. The granular ice portions are significantly higher than those observations from earlier studies, which may indicate a greater amount of snow-ice accretion in the Amundsen Sea than what have been reported previously for Antarctic sea ice elsewhere. Lower columnar texture fractions might indicate little additional congelation growth for most pack ice stations.

The normally low-resolution (one subsample per 10 cm) isotopic measurements were performed for all ice cores. High-resolution isotopic analyses (one subsample per 1 cm) were performed in the 0–10 cm section of core A5. As shown in Figure 4, there is an enriched trend of water isotopes in the 0–10 cm section, which could be due to the diffusion process or growth-rate dependent fractionation (Eicken, 1998). The 0–6 cm layer with negative $\delta^{18}O$ signature should be classified as snow

https://doi.org/10.1017/aog.2020.55 Published online by Cambridge University Press

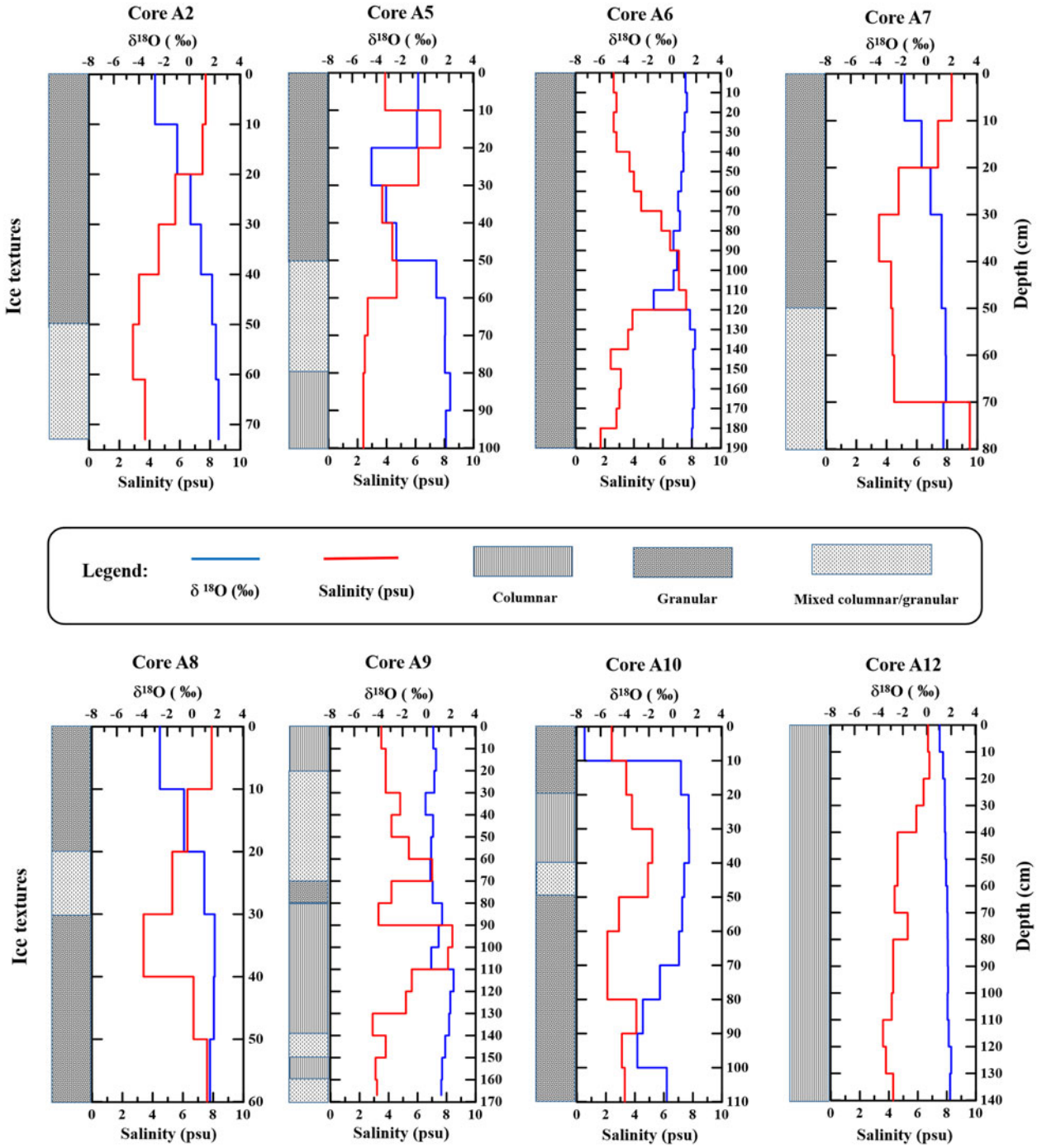

Fig. 3. Ice texture, salinity and oxygen isotope profiles for the eight ice cores collected in the Amundsen Sea.

ice, and the 6–10 cm layer with positive $\delta^{18}O$ signature should be classified as frazil ice. However, the mean $\delta^{18}O$ of the 0–10 cm ice section is − 0.5‰, then the whole 0–10 cm layer would be classified as snow ice. Therefore, the classification approach would provide an upper limit to the contribution of snow ice (Jeffries and others, 1997) due to normally low-resolution isotopic measurements.

Ice textures are also examined for their relationship with salinity and isotope signal (Fig. 5). The boxplot for salinity (Fig. 5a) of the three ice texture classes shows small differences for mean salinity values among the three ice textures. The boxplot for $\delta^{18}O$ (Fig. 5b) shows the granular layers with a lower mean $\delta^{18}O$ signal and a broad range of $\delta^{18}O$ signals. Typically uppermost granular ice layers with negative $\delta^{18}O$ have been interpreted as snow ice and underlying granular layers interpreted as frazil ice. However, in our study, the frazil layers might also possess negative $\delta^{18}O$ signals from the exchange or diffusion processes discussed earlier.

Snow-ice contribution calculations

As shown in Figure 6, $\delta^{18}O$ against δD for all sea ice samples indicates a significant linear relationship: $\delta D = 7.91\delta^{18}O - 0.01$ ($N = 92$; $R^2 = 0.996$). Thus, $\delta^{18}O$ and δD would work equivalently in mass balance calculations using the isotope mixing model for these ice cores. All sea-ice subsamples align on a straight line with a slope very close to the Global Meteoric Water Line $\delta D = 8\delta^{18}O + 10$ (Craig, 1961), which indicates similar growth conditions for all sea-ice stations. The deuterium intercept of the regression equation is close to 0, which indicates evaporation

https://doi.org/10.1017/aog.2020.55 Published online by Cambridge University Press

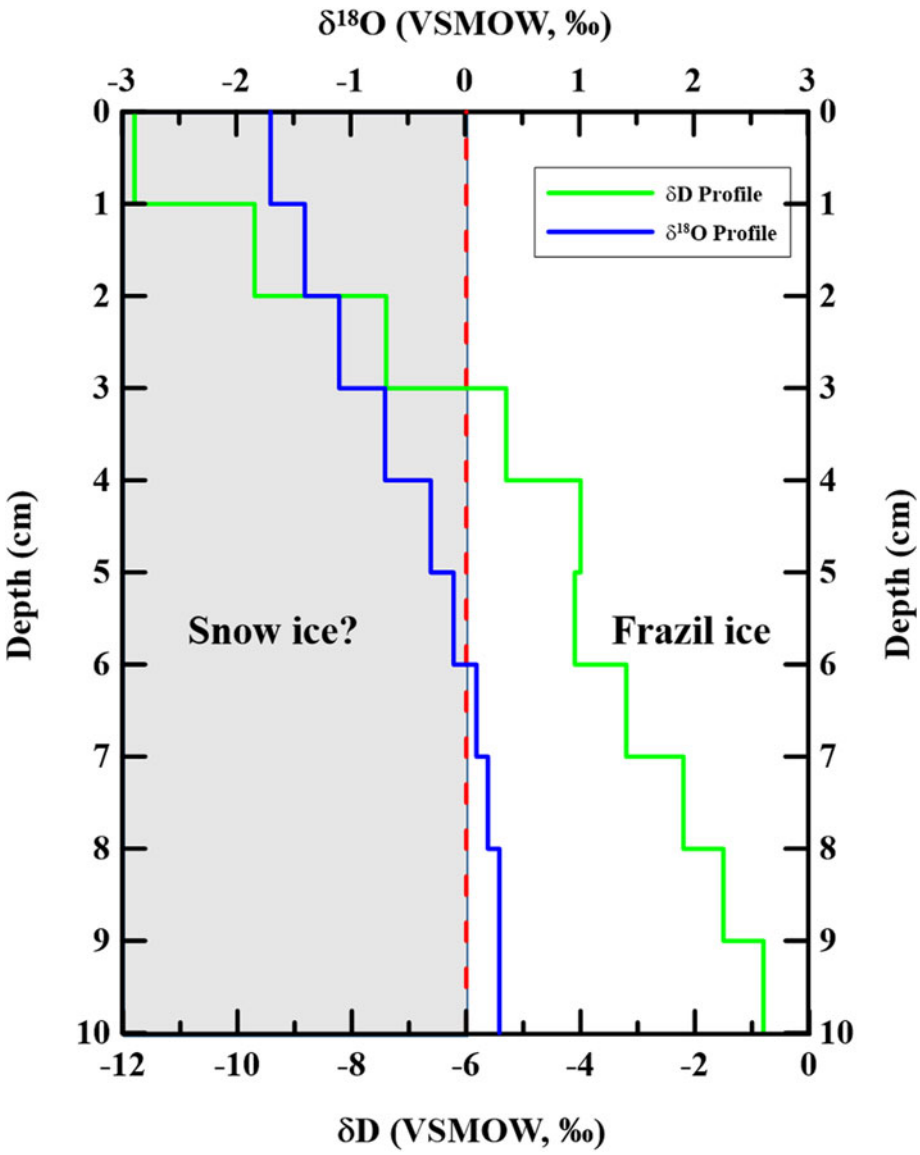

Fig. 4. High-resolution isotopic analyses performed in the 0–10 cm section of core A5.

and other dynamic fractionations are negligible during the growth phase (Souchez and others, 2000). Among our sea-ice sections, the most enriched isotopic values for all ice stations are close to $\delta^{18}O = 2‰$, which could be considered as pure seawater origin signals. The most depleted $\delta^{18}O$ value (− 7.3‰) found at ice station A10 could be considered as snow-ice endmember; however, there is a lack of pure snow-ice signal in other ice stations due to the mixing and diffusion processes.

Isotopic fractionation occurs during freezing, so the solid phase becomes enriched in the heavy isotopes (O'Neil, 1968). The isotopic fractionation during the freezing of seawater leads to elevated $\delta^{18}O$ in the ice phase, and the equilibrium fractionation was determined as 2.8‰ by Beck and Muennich (1988). Seawater had a mean $\delta^{18}O$ value of − 0.5‰ in the Amundsen Sea (derived from Global Seawater Oxygen-18 Database: https://data.giss.nasa.gov/o18data/). The most enriched $\delta^{18}O$ value of basal ice layers is 2.3‰ (Fig. 3), which agrees with the predicted isotopic fractionation very well. Maksym and Jeffries (2001) suggested the effective fractionation coefficient could be a shift in $\delta^{18}O$ of 1–5‰ depending on freezing conditions, which combined effects of the fractionation coefficient, solid to liquid phase change during grain coarsening of snow in the slush, and convective transport of enriched brine out of the slush during freezing. Thus the fractionation coefficient used here might underestimate the net effect of various isotopic exchange processes. However, the most enriched isotopic values for all ice stations could be considered as pure seawater origin signals. Therefore, we directly use the mean with one standard deviation of the most enriched isotopic values for all ice stations as our seawater endmember (after freezing fractionation): $\delta^{18}O = 1.9 \pm 0.4‰ (N = 8)$.

We did not have isotopic measurements of snow/meteoric water samples in our study. To quantify the meteoric-water endmember, the long-term mean isotopic values of annual precipitation were calculated using the Online Isotopes in Precipitation Calculator (OIPC, http://www.waterisotopes.org). The modeled $\delta^{18}O$ and δD of annual precipitation for all ice stations are shown in Figure 7. The modeled $\delta^{18}O$ of annual precipitation for all pack ice stations display similar isotopic signatures (around − 22‰) except the fast ice station A12 with more negative isotopic value (− 29‰) due to its long distance from the moisture source. The mean $\delta^{18}O$ value of meteoric water for all pack ice stations is − 21.9‰. Utilizing the endmembers for seawater (2.3‰) and meteoric water (− 21.9‰), and mass mixing ratios varying from 7:3 to 5:5 for snow-ice mass derived from the typical snow densities (Sturm and others, 1998), we could obtain snow ice with $\delta^{18}O$ values from − 5.0‰ to − 9.8‰. The most depleted $\delta^{18}O$ value (− 7.3‰) of the surface ice section at A10 is the

https://doi.org/10.1017/aog.2020.55 Published online by Cambridge University Press

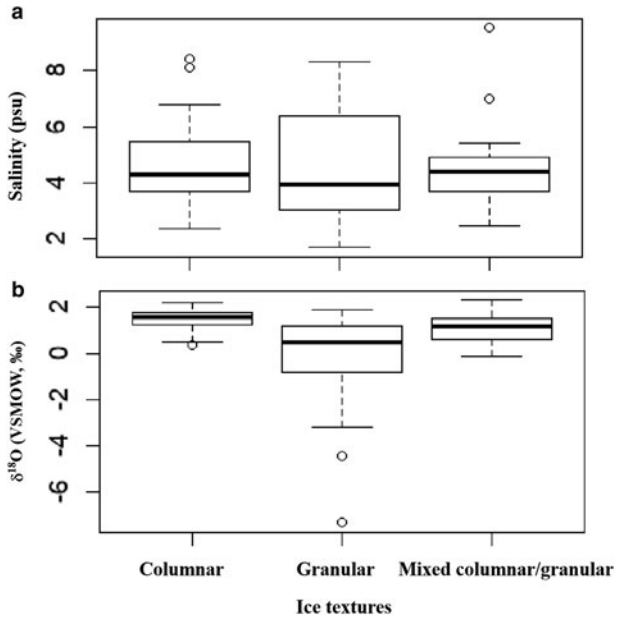

Fig. 5. Boxplot for salinity (a), $\delta^{18}O$ (b) among the three classes of ice textures.

mixture of 60% seawater and 40% of meteoric water. Thus, we can utilize the $\delta^{18}O$ of $-7.3‰ \pm 2.5‰$ as the range of potential values of snow ice (Fig. 7).

Identifying all sea-ice layers with negative isotope signature ($\delta^{18}O < 0$) as snow ice, we calculated total percentages of core length containing snow ice (P_{SI}) for all pack ice cores. Utilizing isotope mixing model in mass-balance calculations, we calculated the snow-ice fraction (F_{SI}) for all pack ice cores based on equation (3), and meteoric-water fraction (F_M) for all ice cores based on equation (4). There should be no snow-ice formation at fast ice station A12, then only meteoric-water fraction was calculated at A12. The water balance calculations utilized the IsoError single-isotope two-source model described by Phillips and Gregg (2001). This mixing model calculates means and standard errors of source proportional contributions to a mixture using stable isotope analyses.

These apportionment results of snow ice (P_{SI} and F_{SI}) for each ice core are presented in Table 2. The P_{SI} results using the standard classification method show a broad range of change from 5 to 50%, with a thickness-weighted average of 22.9%. In contrast, the F_{SI} results for pack ice calculated from our updated isotope mixing model vary from 10.2 to 29.6%, with a thickness-weighted average of 15.9%. Compared with the previous classification method, we feel our updated mixing model returned more consistent and reasonable snow-ice contribution results. Five ice cores (A2, A5, A7, A8 and A10) yield $P_{SI} > F_{SI}$, which might be due to the vertical mixing process or low resolution of sampling. Thus, many slightly negative $\delta^{18}O$ layers could be mixtures of the snow-ice and seawater signals. Only two ice cores (A6 and A9) yield $P_{SI} < F_{SI}$, which indicates that the diffusion processes during the refreezing of snow ice might modify the isotopic signatures of the snow ice and underlying ice layers, then the positive $\delta^{18}O$ layers could also contain some degree of snow-ice signals. Another possibility is that the isotope mixing model would overestimate snow-ice fraction due to the incorporation of falling snow through frazil accumulation. Therefore, the classification approach might provide not only an upper limit to the amount of the snow ice (Jeffries and others, 1997) but also a lower limit of snow-ice contribution for some ice cores.

The derived meteoric-water fraction (F_M) for each ice core is also presented in Table 2. The F_M fractions for pack ice vary from 3.9 to 11.3%, with a thickness-weighted average of 6.2%. The F_M fractions are nearly 40% of the F_{SI} fractions for all pack ice stations, which agrees with the assumption that meteoric water occupied from 30 to 50% the snow-ice during the freezing of a slush layer (Maksym and Jeffries, 2001). However, the F_M fractions account for 20–100% of the P_{SI} fractions, which contradicts the derived mass mixing ratio based on the typical snow densities (Sturm and others, 1998). Cores A6 and A9 have low P_{SI} and almost equal F_M, but the snow/meteoric water could not occupy that high fraction for the snow-ice layers. Thus, many positive $\delta^{18}O$ layers in these two cores might also have some F_M fractions due to the diffusion process. The F_M fraction for the fast ice station A12 is 1.0%, which indicated limited incorporation of falling snow through the congelation ice growth.

We found the snow-ice contributions (Table 2) are independent of the measured snow depths at the time of sampling (Table 1). Even though only trace snow was observed at core A2, our isotope mixing model still returned 14.5% of sea-ice mass as snow ice. Thus, the measured snow depth at the time of sampling may not indicate snow-ice formation previously, and snow depth may be a poor indicator of total snow accumulation (Maksym and Markus, 2008). The possible reasons include thick sea ice would not flood with a larger amount of snow or thin ice flooded even with a small amount of snow; the deep snow with slush layers observed in summer does not necessarily imply substantial snow-ice formation previously or erased any relationship from previous winter.

Comparison with previous investigations

Snow ice has been observed in all regions and seasons in Antarctic pack ice (Lange and others, 1990; Allison and Worby, 1994; Eicken and others, 1994; Jeffries and others, 1994, 1997, 2001). However, these studies reported highly variable contributions of snow ice to the total sea-ice thickness: ranging from only 7% of the ice thickness in the Weddell Sea (Lange and others, 1990) to as high as 36% in the northern Bellingshausen/Amundsen Seas (Jeffries and others, 2001). The snow-ice contributions varied seasonally in the same region (Allison and Worby, 1994). The contribution of snow ice in the winter (Jeffries and others, 1997) was greater than that in the summer (Jeffries and others, 1994) for pack ice in the Bellingshausen Sea. There was an elevated snow-ice contribution for second-year ice than first-year ice (Eicken and others, 1994). However, there is almost no in situ data available along the southern Amundsen Sea until now. Our updated isotope mixing model indicated snow-ice contributions in the southern Amundsen Sea range from 10.2 to 29.6% with an average of 15.9%, which lie within the range of previously reported results around Antarctica.

The modeling of snow-ice thickness in the Antarctic produced the thinnest snow ice in the Weddell Sea, whereas the thickest snow ice was predicted along the coast in the Amundsen Sea (Maksym and Markus, 2008). However, our mixing model returns moderate snow-ice contribution in the southern Amundsen Sea, which contradict with the modeling results predicted by Maksym and Markus (2008). It is possible that the model might not be well-enough defined yet due to the limits of the snow depth product or the uncertainty of processes that control snow accumulation on sea ice. Our results suggest, however, the quantities of snow ice might not be significantly higher than other regions despite more snowfall in the Amundsen Sea. Comparing to previous studies (Jeffries and others, 1994, 2001) in the Amundsen Sea, the snow-ice contributions in our study are much lower even though the meteoric-water contributions are comparable with those of the previous studies. Our isotope mixing models returned meteoric-water and snow-ice

https://doi.org/10.1017/aog.2020.55 Published online by Cambridge University Press

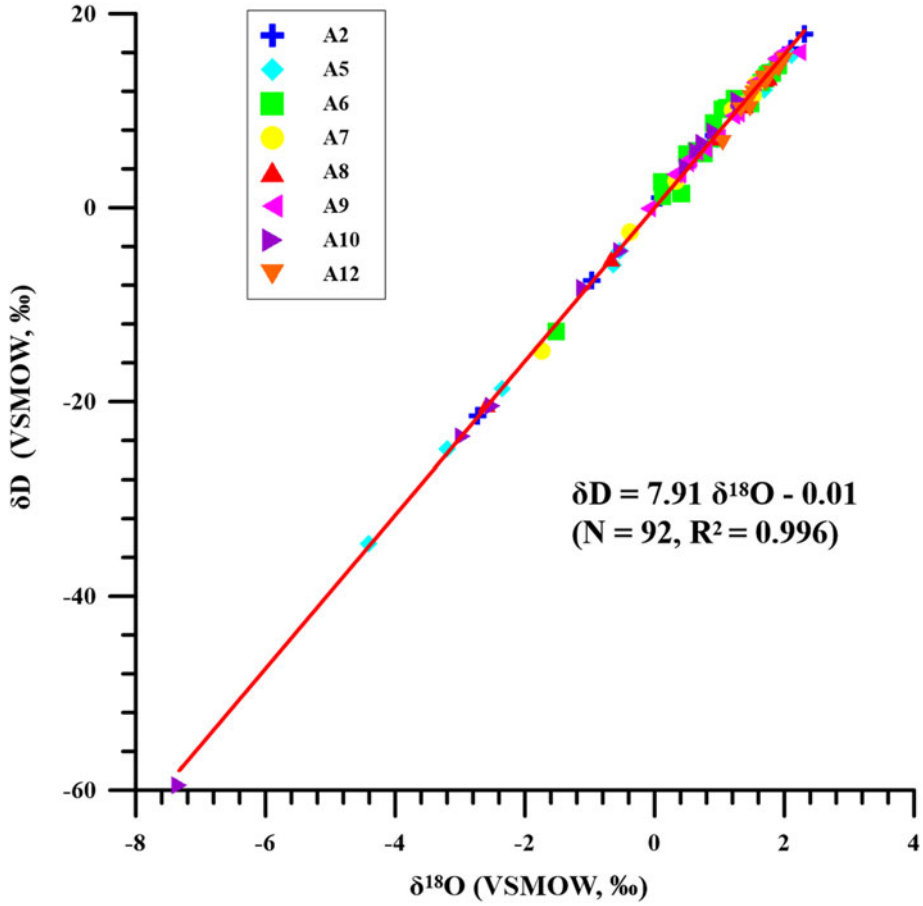

Fig. 6. Cross plot of $\delta^{18}O$ against δD for the sea-ice samples of the eight ice cores collected during the OSO1011 expedition. The best-fitting regression line for all sea-ice samples is shown in the figure.

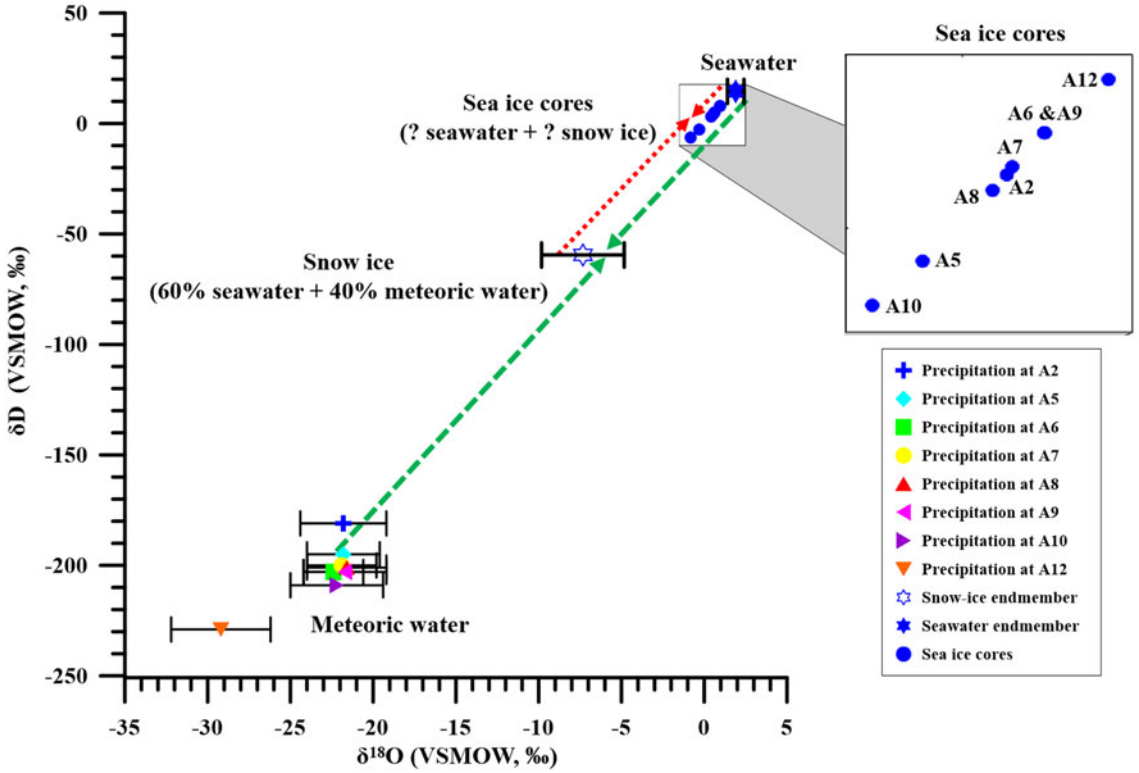

Fig. 7. Cross plot of $\delta^{18}O$ against δD for the thickness-weighted means of ice cores, and the endmembers for meteoric water, snow ice and seawater. The modeled isotopes in annual precipitation for the eight ice stations were calculated using the Online Isotopes in Precipitation Calculator (OIPC, http://www.waterisotopes.org). The green dashed mixing lines partition contributions of meteoric water and seawater for snow ice, and the red dashed mixing lines partition contributions of snow ice and seawater for all ice cores. The error bars of $\delta^{18}O$ for these endmembers are also shown in the figure.

https://doi.org/10.1017/aog.2020.55 Published online by Cambridge University Press

Table 2. Summary of the ice cores with the mean and range of $\delta^{18}O$, thickness percentages of core length containing snow ice (P_{SI}), snow-ice fractions (F_{SI}), meteoric-water fractions (F_M). F_{SI} and F_M presented here are the thickness percentages (mean ± standard error) calculated by the isoError single-isotope two-source model (https://www.epa.gov/eco-research/stable-isotope-mixing-models-estimating-source-proportions)

Core No.	Core length cm	$\delta^{18}O$ range ‰	Mean $\delta^{18}O$ ‰	P_{SI} %	F_{SI} %	F_M %
A2	73	(−2.73, 2.31)	0.57	27	14.5 ± 2.0	5.6 ± 0.6
A5	100	(−4.41, 2.11)	−0.30	50	23.9 ± 2.6	9.3 ± 0.6
A6	190	(−1.52, 1.90)	0.96	5	10.2 ± 1.8	3.9 ± 0.6
A7	80	(−1.74, 1.55)	0.63	25	13.8 ± 2.0	5.3 ± 0.6
A8	60	(−2.59, 1.76)	0.42	33	16.1 ± 2.1	6.3 ± 0.6
A9	167	(−0.10, 2.22)	0.95	6	10.3 ± 1.8	4.0 ± 0.6
A10	110	(−7.33, 1.32)	−0.82	45	29.6 ± 3.1	11.3 ± 0.7
A12	140	(1.05, 2.00)	1.62	NA	NA	1.0 ± 0.5
Total	920	(−7.33, 2.31)	0.61	22.9	15.9	6.2

contributions with reasonable ratios. We speculate the previous studies may have overestimated the snow-ice contributions, due to the possible misclassification of ice layers with slightly negative isotope values utilizing the standard classification method.

These observed spatial or temporal variations of snow-ice contributions might be attributed to different meteorological conditions and surface topography amongst these ice stations. The pack ice with greater snow accumulation and more dynamic environments favors flooding and snow-ice formation (Jeffries and Adolphs, 1997). However, parts of the inconsistency for snow-ice contributions might be attributed to the significant error of standard practice of snow-ice identification. There is a lack of understanding of controlling factors on the evolution of snow ice, and in-situ measurements and isotopic analyses of ice cores are very limited. We suggest that more ice cores in the Antarctic with differing meteorological conditions and surface topography should be examined using the updated isotopic mixing model in future research.

Conclusions

Depth profiles of stable isotopes, salinity and ice texture were described to serve as illustrations of snow-ice formation and the evolution of pack ice in the Amundsen Sea. We utilized an updated oxygen isotope mixing model to determine the snow-ice contribution in the mass balance. The main conclusions drawn are:

(1) The standard procedure to calculate the percentages of core length containing meteoric water might be biased due to the normally low-resolution isotopic measurements for ice cores. The mixing and diffusion processes during the flooding and refreezing of snow ice may also modify its isotopic signature. The previous snow-ice identification method might provide not only an upper limit to the amount of the snow ice but also a lower limit of snow-ice contribution for some ice cores.
(2) The water balance calculations utilized the IsoError single-isotope two-source model. The most enriched and most depleted $\delta^{18}O$ values represent the best estimate of endmembers of 'seawater' and 'snow ice' respectively. The derived snow-ice contributions for pack ice range from 10.2 to 29.6% with a thickness-weighted average of 15.9% in the Amundsen Sea. The meteoric-water fractions for pack ice range from 3.9 to 11.3% with an average of 6.2%.
(3) The meteoric water has occupied 40% of snow-ice mass for all ice stations using our isotope mixing model, whereas the meteoric water has highly variable fractions in the snow-ice mass utilizing the classification approach. Comparing to previous studies, the more consistent and reasonable snow-ice contribution results in this study verified the validity of our isotope mixing model. Due to only a small sample size of cores obtained in our study, more ice cores in the Antarctic need to be examined using our refined isotope mixing model in future research.

Contribution statement. BW collected the ice cores and provided field observations of sampling conditions. SFA conducted the cold room analyses of ice structure and salinity on returned cores. LT and YG conducted water isotope analyses and analyzed the isotope records for snow-ice contributions. LT wrote the first draft of the paper and all authors contributed to interpretations and final writing and editing.

Supplementary material. Data of stable isotopes, salinity, and ice texture used in this study can be found at U.S. Antarctic Program Data Center (USAP-DC): http://www.usap-dc.org/view/dataset/600106.

Acknowledgements. SFA acknowledges the support of NASA through the NASA Center on Advanced Measurements in Extreme Environments at UTSA (NASA CAMEE #80NSSC19M0194) during the conduct of this research. This project was also funded (in part) by the University of Texas at San Antonio (UTSA), Office of the Vice President for Research, the Amy Shelton and V.H. McNutt endowment, and the Center for Water Research at UTSA.

References

Ackley SF and Sullivan CW (1994) Physical controls on the development and characteristics of Antarctic sea ice biological communities–a review and synthesis. *Deep-Sea Research Part I: Oceanographic Research Papers* **41**, 1583–1604. doi: 10.1016/0967-0637(94)90062-0.

Allison I and Worby A (1994) Seasonal changes of sea-ice characteristics off East Antarctica. *Annals of Glaciology* **20**, 195–201. doi: 10.3189/1994AoG20-1-195-201.

Arrigo KR, Worthen DL, Lizotte MP, Dixon P and Dieckmann G (1997) Primary production in Antarctic sea ice. *Science* **276**, 394–397. doi: 10.1126/science.276.5311.394.

Beck N and Muennich KO (1988) Freezing of water: isotopic fractionation. *Chemical Geology* **70**, 168. doi: 10.1016/0009-2541(88)90693-6.

Craig H (1961) Isotopic variations in meteoric waters. *Science* **133**(3465), 1702–1703. doi: 10.1126/science.133.3465.1702.

Drinkwater MR and Lytle VI (1997) ERS 1 radar and field-observed characteristics of autumn freeze-up in the Weddell Sea. *Journal of Geophysical Research-Part C-Oceans* **102**, 12593–12608. doi: 10.1029/97JC00437.

Eicken H (1998) Deriving modes and rates of ice growth in the Weddell Sea from microstructural, salinity and stable-isotope data. *Antarctic sea ice: Physical Processes, Interactions and variability, Antarctic Research Series* **74**, 89–122. doi: 10.1029/AR074p0089.

Eicken H, Lange MA and Wadhams P (1994) Characteristics and distribution patterns of snow and meteoric ice in the Weddell Sea and their contribution to the mass balance of sea ice. *Annales de Geophysique* **12**, 80–93. doi: 10.1007/s00585-994-0080-x.

Fritsen C, Lytle V, Ackley S and Sullivan C (1994) Autumn bloom of Antarctic pack-ice algae. *Science* **266**, 782–784. doi: 10.1126/science.266.5186.782.

Golden K, Ackley S and Lytle V (1998) The percolation phase transition in sea ice. *Science* **282**, 2238–2241. doi: 10.1126/science.282.5397.2238.

Granskog MA and 6 others (2017) Snow contribution to first-year and second-year Arctic sea ice mass balance north of Svalbard. *Journal of Geophysical Research: Oceans* **122**, 2539–2549. doi: 10.1002/2016JC012398.

Jeffries MO and Adolphs U (1997) Early winter ice and snow thickness distribution, ice structure and development of the western Ross sea pack ice between the ice edge and the Ross Ice Shelf. *Antarctic Science* **9**, 188–200. doi: 10.1017/S0954102097000242.

Jeffries MO, Krouse HR, Hurst-Cushing B and Maksym T (2001) Snow-ice accretion and snow-cover depletion on Antarctic first-year sea-ice floes. *Annals of Glaciology* **33**, 51–60. doi: 10.3189/172756401781818266.

Jeffries MO, Morris K, Weeks WF and Worby AP (1997) Seasonal variations in the properties and structural composition of sea ice and snow cover in the Bellingshausen and Amundsen Seas, Antarctica. *Journal of Glaciology* **43**, 138–151. doi: 10.3189/S0022143000002902.

Jeffries MO, Shaw RA, Morris K, Veazey AL and Krouse HR (1994) Crystal structure, stable isotopes (δ^{1}8O), and development of sea ice in the Ross, Amundsen, and Bellingshausen seas, Antarctica. *Journal of Geophysical Research: Oceans* **99**, 985–995. doi: 10.1029/93JC02057.

Lange M and Hubberten HW (1992) Isotopic composition of sea ice as a tool for understanding sea ice processes in the polar regions. In Maeno, N and Hondoh, T eds. *Physics and chemistry of ice*. Hokkaido Univ Pr, Sapporo, 399–405.

Lange MA, Schlosser P, Ackley SF, Wadhams P and Dieckmann GS (1990) ^{1}8O concentrations in sea ice of the Weddell sea, Antarctica. *Journal of Glaciology* **36**, 315–323. doi: 10.3189/002214390793701291.

Lytle VI and Ackley SF (2001) Snow-ice growth: a fresh-water flux inhibiting deep convection in the Weddell sea, Antarctica. *Annals of Glaciology* **33**, 45–50. doi: 10.3189/172756401781818752.

Maksym T and Jeffries MO (2001) Phase and compositional evolution of the flooded layer during snow-ice formation on Antarctic sea ice. *Annals of Glaciology* **33**, 37–44. doi: 10.3189/172756401781818860.

Maksym T and Markus T (2008) Antarctic sea ice thickness and snow-to-ice conversion from atmospheric reanalysis and passive microwave snow depth. *Journal of Geophysical Research: Oceans* **113**, C02S12. doi: 10.1029/2006JC004085.

Maksym T, Stammerjohn SE, Ackley S and Massom R (2012) Antarctic Sea ice– A Polar Opposite. *Oceanography* **25**, 140–151. doi: 10.5670/oceanog.2012.88.

Massom RA and 10 others (2001) Snow on Antarctic sea ice. *Reviews of Geophysics* **39**, 413–445. doi: 10.1029/2000RG000085.

O'Neil JR (1968) Hydrogen and oxygen isotope fractionation between ice and water. *Journal of Physical Chemistry* **72**, 3683–3684. doi: 10.1021/j100856a060.

Parkinson CL (2019) A 40-y record reveals gradual antarctic sea ice increases followed by decreases at rates far exceeding the rates seen in the Arctic. *Proceedings of the National Academy of Science* **116**, 14414–14423. doi: 10.1073/pnas.1906556116.

Phillips DL and Gregg JW (2001) Uncertainty in source partitioning using stable isotopes. *Oecologia* **127**(2), 171–179. doi: 10.1007/s004420000578).

Souchez R and 5 others (2000) A kinetic isotope effect during ice formation by water freezing. *Geophysical Research Letters* **27**(13), 1923–1926. doi: 10.1029/2000GL006103.

Sturm M, Morris K and Massom R (1998) The winter snow cover of the West Antarctic pack ice: its spatial and temporal variability. *Antarctic sea ice: physical processes, interactions and variability, Antarctic Research Series* **74**, 1–18. doi: 10.1029/AR074p0001.

Tian L and 5 others (2018) Stable isotope clues to the formation and evolution of refrozen melt ponds on Arctic sea ice. *Journal of Geophysical Research: Oceans* **123**, 8887–8901. doi: 10.1029/2018JC013797.

Xie H, Tekeli AE, Ackley SF, Yi D and Zwally HJ (2013) Sea ice thickness estimations from ICESat Altimetry over the Bellingshausen and Amundsen Seas, 2003–2009. *Journal of Geophysical Research: Oceans* **118**, 2438–2453. doi: 10.1002/jgrc.20179.

https://doi.org/10.1017/aog.2020.55 Published online by Cambridge University Press